The Impact of Strain Reversal on Microstructure Evolution and Orientation Relationships in Ti-6Al-4V with an Initial Alpha Colony Microstructure

K. MUSZKA, M. LOPEZ-PEDROSA, K. RASZKA, M. THOMAS, W.M. RAINFORTH, and B.P. WYNNE

The effect of forward and reverse torsion on flow behavior and microstructure evolution, particularly dynamic and static spheroidization, on Ti-6Al-4V with an alpha lamella colony microstructure was studied. Testing was undertaken sub beta transus [1088 K (815 °C)] at strain rates of either 0.05 or 0.5 s^{-1}. Quantitative metallography and electron back scatter diffraction has identified that a critical monotonic strain (ε_c) in the range of 0.3 to 0.6 is required to initiate rapid dynamic spheroidization of the alpha lamella. For material deformed to strains below ε_c and then reversed to a zero net strain the orientation relationships between alpha colonies are close to ideal Burgers, enabling prior beta grains to be fully reconstructed. Material deformed to strains greater than ε_c and reversed lose Burgers and no beta reconstruction is possible, suggesting ε_c is the strain required to generate break-up of lamella. Static spheroidization is, however, sensitive to strain path around ε_c. Annealing at 1088 K (815 °C) for 4 hours for material subjected to 0.25 forward + 0.25 forward strain produces 48 pct spheroidized grains while material with 0.25 forward + 0.25 reverse strain has 10 pct spheroidization. This is believed to be a direct consequence of different levels of the stored energy between these two strain paths.

DOI: 10.1007/s11661-014-2590-9

I. INTRODUCTION

IN the processing of as-cast billet during hot working of Ti alloys, the sub beta transus breakdown of beta recrystallized as-transformed microstructure to a fine grain two-phase equiaxed microstructure, known as spheroidization,[1,2] is an important technological process for producing a highly formable semi-finished product suitable for subsequent hot working processes. Breakdown of the as-transformed alpha colony or basketweave structure during working in alpha + beta phase field can occur dynamically (during deformation) or statically (after deformation) with the extent of spheroidization dependent on the applied level of strain,[3] the temperature of deformation,[3] the time held at temperature,[3] and the applied strain path.[1–3] The main driving force for dynamic spheroidization is the formation of intense shear bands within alpha lamella. The formation of such high energy alpha/alpha interfaces in contact with beta platelets is postulated to give rise to surface tension driven penetration of the alpha plates by the beta phase.[5] It is therefore not surprising that non-monotonic types of deformation (*e.g.*, reversed torsion, tension/compression), which change the intensity of shear bands within the alpha lamella, have also been shown to significantly reduce the rate of spheroidization compared to equivalent monotonic strains.[4] Thus understanding strain path effects on spheroidization is critical for optimization of the forging process, which is highly non-linear and involves continuous strain path changes,[3] which, in turn, could lead to a substantial cost reduction in the widely used alpha + beta alloys. However, most of the recent strain path research has been performed at very low strain rates (that are far from the real industrial processes) and focused only on quantification the extent of spheroidization. Thus, in this work an additional objective was to study the reversibility of the Burgers orientation relationships that are inherited from the beta to alpha phase transformation. Identification of an existence of a threshold strain, beyond which the return of the original as-transformed Burgers relationship is no longer possible, may be crucial for understanding the critical straining

K. MUSZKA, Assistant Professor, is with the Faculty of Metals Engineering and Industrial Computer Science, AGH University of Science and Engineering, Mickiewicza 30, 30-059 Kraków, Poland, and also with the Department of Materials Science and Engineering, The University of Sheffield, Sir Robert Hadfield Building, Mappin St, Sheffield S1 3JD, U.K. Contact e-mail: muszka@agh.edu.pl M. LOPEZ-PEDROSA, formerly Research Associate with the Department of Materials Science and Engineering, The University of Sheffield, is now Scientific Officer with the Itasca UK, 5 Claremont Buildings, Shrewsbury SY1 1RJ, U.K. K. RASZKA, formerly Student with the Department of Materials Science and Engineering, The University of Sheffield, and also with the Faculty of Metals Engineering and Industrial Computer Science, AGH University of Science and Engineering, is now Metallurgical Engineer with the Firth Rixson River Don, Milford St, Sheffield, S9 2LD, U.K. M. THOMAS, UK R&D Manager, is with the TIMET UK LTD, PO Box 704, Witton, Birmingham, B6 7UR, U.K. W.M. RAINFORTH and B.P. WYNNE, Professors, are with the Department of Materials Science and Engineering, The University of Sheffield.

Manuscript submitted November 12, 2013.
Article published online September 30, 2014

conditions for the onset of dynamic spheroidization. Hence, the main aim of the present study is to understand the impact of strain reversal on the interaction between the stability of the Burgers relationship and spheroidization under industrially relevant process conditions.

II. EXPERIMENTAL

In order to assess the effect of strain reversal on the amounts of fractions dynamically and statically spheroidized, isothermal forward/reverse torsion tests were conducted using the torsion component of the special-purpose arbitrary strain-path rig at The University of Sheffield (UK). The material used in this work was a commercially produced α/β titanium alloy, Ti-6Al-4V, provided by TIMET UK Ltd. The material was received as a hot-rolled (above the beta transus temperature) 30-mm-diameter bar, which had been mill annealed at 973 K (700 °C) for 2 hours, resulting in a microstructure comprising of equiaxed-α and transformed β structure. Its composition (in weight percent) was determined to be 6.6Al/4.1V/0.2O/0.06C/0.07N/0.004H, the balance being Ti with a nominal β-transus temperature of 1268 K (995 °C). Typical cylindrical torsion samples with strain gage diameter of 10 mm and strain gage length of 18 mm were machined out of the provided bars. In order to produce a colony α microstructure similar to that generated in an industrially sized beta recrystallized billet,[4] a multiple-stage heat treatment was carried out on these samples prior to mechanical testing—Figure 1.

For the specimen heating, induction coil was used and sample's temperature was monitored and controlled by a thermocouple that was inserted in a hole drilled at the shoulder position of the gage section, 45 deg toward the center of the specimen's gage. The initial heat treatment consisted of 6 minutes holding at 1088 K (815 °C) followed by 1 minute holding at 1313 K (1040 °C) followed by 2 minutes holding at 1223 K (950 °C), and, finally 10 minutes holding at 1088 K (815 °C). After heat treatment specimens were cooled to room temperature with a cooling rate of 4 °C s^{-1}. The microstructure produced by this heat treatment is presented in Figure 2(a). It consists of equiaxed prior-β grains containing a transformed structure of colony α. The prior-β grain size is around 110 μm, the mean α-lamella thickness is around 1 μm, and the prior-β grain boundaries were decorated with a 2-μm-thick layer of grain boundary α. It should also be noted that this heat treatment generated an alpha case no greater than 20 μm on the surface of the test samples. Figure 2(b) shows the crystallographic texture analysis result performed on the heat-treated and water-quenched material using the Electron Backscatter Diffraction (EBSD) technique. It is characterized by a relatively strong rolling texture *e.g.*, the (0002) α-phase pole figure (Figure 2(b)) revealed a strong basal-fiber-texture component parallel to the bar axis.

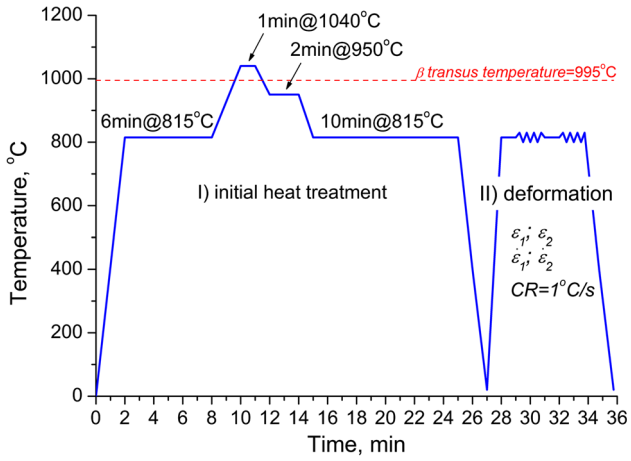

Fig. 1—Schematic summary of heat treatment and deformation schedule applied in the present work.

The specimens were then reheated to the deformation temperature [1088 K (815 °C)] and deformed in torsion according to the deformation routes that are summarized in Table I. The torque–twist angle data was during torsional deformation and subsequently converted into shear stress–shear strain according to the method proposed by Fields and Backofen[6] and then, into true stress–true strain by applying Von Mises criterion. In order to look at the effect of strain path on the extent of static spheroidization, post deformation annealing was additionally applied for deformation routes 1 and 2.

For microstructural study, optical, scanning electron microscopy, and electron backscatter diffraction (EBSD) mapping were conducted at the specimen's cross section perpendicular to the longitudinal axis. A linear increase in the effective strain from the sample center to the surface allowed a range of strains to be studied in each sample. In this way, the relationship between the applied strain and fraction spheroidized over a range of strains was assessed using a limited number of tests. In order to assess the volume fractions of spheroidized alpha grains, spheroidization was taken to be an alpha-phase morphology with an aspect ratio of less than ≈2:1. From the measurements, plots of fraction spheroidized versus effective strain were constructed.

The EBSD data were collected using a FEI field emission gun scanning electron microscope (FEGSEM) equipped with a HKL Nordlys CCD camera. HKL Channel 5 software package was used for both data acquisition and analysis.

Based on the EBSD data, parent beta microstructure was reconstructed utilizing the approach described in Reference 7. It is well known that phase transformation in Ti-6-4 alloys occurs with specific orientation relationship between the precursor BCC beta and transformed HCP alpha phase,[8,9] and it is generally governed by the following Burgers relationship:

$$(101)_\beta \Big\| (0001)_\alpha, \quad [11\bar{1}]_\beta \Big\| [11\bar{2}0]_\alpha. \qquad [1]$$

Because of crystal symmetry, there are 12 possible alpha orientations that can transform from a single parent beta

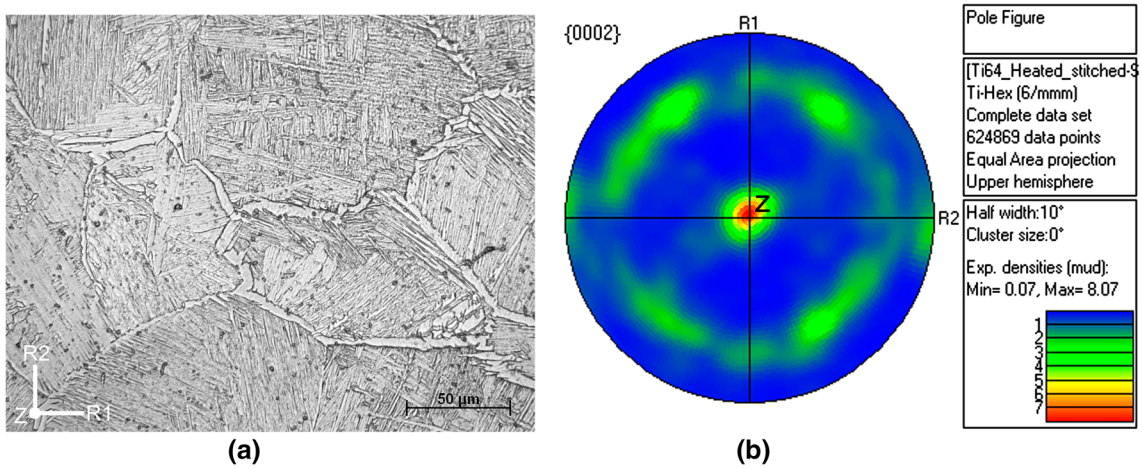

Fig. 2—(*a*) Optical micrograph of water-quenched microstructure after initial heat treatment (see Fig. 1). (*b*) α-phase (0002) pole figure of the heat-treated and water-quenched material. The rolling direction of the initial material was the same as the shear direction Z of the torsion tests and is normal to R1, R2 plane indicated in the pole figure.

Table I. Deformation Routes Applied in the Present Work

Deformation Route	1st Pass	2nd Pass	Total Equivalent Strain	Net Strain	Strain Rate (1/s)	Post-deformation Heat Treatment	CR (°C s^{-1})
1a	0.25F	0.25F	0.5	0.5	0.5	—	1
1b						4 h hold @ 1088 K (815 °C)	
2a	0.25F	0.25R	0.5	0	0.5	—	
2b						4 h hold @ 1088 K (815 °C)	
3	1F	1R	2	0	0.05	—	

F: forward strain; *R*: reverse strain at equivalent radius of 0.724R.[10]

grain, *i.e.*, there are 12 variants. There is no variant selection in a parent grain when the volume fractions corresponding to each of the 12 inherited orientation are equal. However in Ti alloys, hot deformation above the beta transus has been reported to lead to transformation with variant selection.[8] Based on this, it is possible to reconstruct the beta phase from room temperature phase when no deformation nor post deformation heat treatment that could destroy the Burgers relationship have occurred. In the current approach, the angle of 3 deg has been used as a minimum tolerance angle to define colonies that originate from the same parent beta grain.

III. RESULTS AND DISCUSSION

In the first part of the present work, effect of strain path change on flow behavior was studied. Figure 3 summarizes the flow curves recorded for deformation routes 1a and 2a. The rotation angle of each deformation pass here was 137 deg and all tests were conducted at a constant angular speed of 224 deg s^{-1}. According to Barraclough *et al.*,[10] this would produce a von Mises equivalent strain of 0.25 for each pass and a constant equivalent strain rate of 0.5 s^{-1} at the effective radius, which is 72.4 pct of the total gage radius. This method helps to minimize the complexity of converting the recorded machine torque and rotation angle data into flow stress and strain.

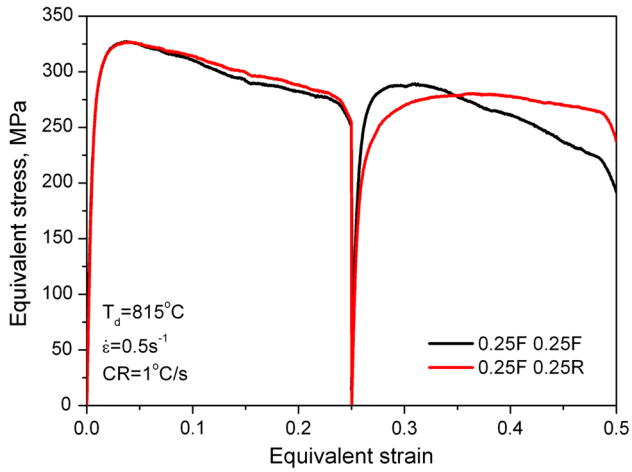

Fig. 3—Flow curves calculated from torque–angle data for deformation routes 1a and 2a. Measurements were taken from the areas corresponding to the total equivalent strain of 0.5 from the plane parallel to the specimen's cross section.

It can be observed that, after the strain reversal, the sample after deformation route 2a was characterized by a lower peak stress and a weaker softening behavior than the sample deformed with the route 1a. The lower peak on the curve can be attributed to the Bauschinger effect that occurs during reversal of the direction of

straining. It is caused by the rearrangement of the dislocation structure—especially removal of geometrically necessary dislocations.[11,12] It can be expected that this then leads to a lower dislocation density and less pronounced microband formation within alpha platelets.[1] As a direct consequence, kinking of the alpha lamellas is more difficult, and thus, dynamic spheroidization process would be expected to be significantly slowed down. In terms of flow softening behavior itself, it can be considered as an effect of both deformation heating and microstructural changes.[7] Because in the studied case, the deformation heating effects were comparable in the two deformation routes, the change in the flow softening rate can be then attributed to the microstructural changes *i.e.*, reduced rate of alpha lammella breakdown. This observation is also consistent with the flow curve recorded for deformation route 3—shown in Figure 4—where flow softening is observed only to the certain strain, that is followed by the plateau observed on the stress curve. No further softening after reaching certain strain would then suggest that the complete dynamic spheroidization has occurred. Additionally, in this case, much lower stress level after complete strain reversal can not be attributed to the Bauschinger effect itself due to much higher strain in the first deformation pass, and microstructural changes due to the breakdown of initial microstructure.

Assessment of the progress of spheroidization of the alpha platelets after deformation routes 1a and 2a was made via comparison of micrographs, obtained using scanning electron microscope with a backscatter electron detector, that are summarized in Figure 5. In the all presented BSE micrographs, darker areas represent alpha phase and bright matrix is a beta phase. It can be seen that in the area of the specimen where strain was zero, the microstructure consists of alpha lamellar structure that looks similar to that observed in the undeformed sample (see Figure 2(a)). The thickness of the alpha lamella is about 1 μm and there is no sign of dynamic spheroidization occurring. In the region where the total equivalent strain was 0.5, it is quite clear that in the case of the forward-forward deformation (route 1a)

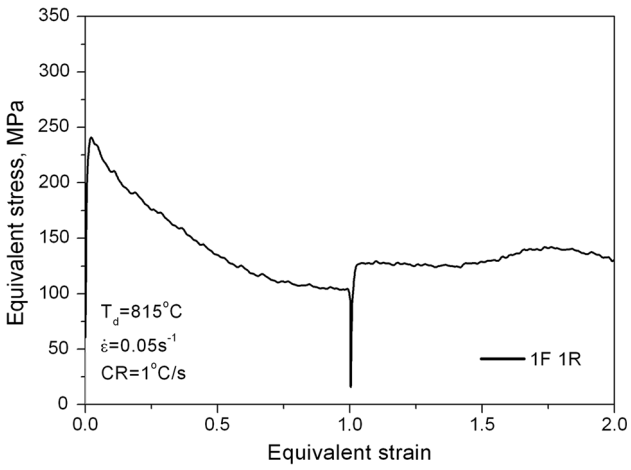

Fig. 4—Flow curve recorded during torsion deformation with deformation route 3 (strain 1F + 1R).

some spheroidized alpha grains can be found, whereas in the case of forward reverse (route 2a) the spheroidization process was very limited.

Microstructures observed along the specimen's radius after application of higher strain and reversal (deformation 3) are presented in Figure 6. By studying the local microstructures and relating them to the corresponding total local strains, it was possible to assess the effect of the amount of applied strain on the progress and rate of dynamic spheroidization process. It can be seen from Figure 7 that the rate of dynamic spheroidization is split into three parts: (1) for total strains up to 0.6 (0.3 forward to 0.3 reverse) the spheroidization rate is constant and low at about 1.6 pct spheroidization/0.1 strain, (2) between total strains of 0.6 and 1.2 there is a rapid but non-constant increase in spheroidization rate, and (3) beyond a total strain of 1.2 to complete spheroidization where there is a constant spheroidization rate of 7.9 pct spheroidization/0.1 strain, which is significantly higher than that in part 1. This would suggest that there is a critical monotonic threshold strain in the range of 0.3 to 0.6 to initiate rapid spheroidization, which is consistent with the flow curve presented above in Figure 4, where a monotonic strain of 0.6 corresponds to the end of flow softening. Figure 5(c) highlights the possible reason for the strain range observed in part 2. Here, there are regions of high levels of spheroidization and regions which are equivalent to as-transformed lamella. These individual regions appear to correlate with alpha-colonies suggesting that some alpha colony orientations require less strain than others to initiate spheroidization but all colonies will have begun to spheroidize by a monotonic strain of $\varepsilon_f = 0.6$.

In order to study the effect of strain path on static spheroidization, post-deformation annealing was additionally applied in samples deformed with deformation routes 1 and 2. It is known that the majority of the static spheroidization occurs as a result of coarsening processes such as Ostwald ripening and termination migration.[5] In the current work, the coarsening process itself was observed, however, it is not possible to identify between the possible mechanisms. Figure 7 shows microstructures taken in the same areas as those presented in Figure 5 for the material that was annealed after deformation at 1088 K (815 °C) for 4 hours. In the areas where there was no strain (Figures 7(a) and (c)), there appears to be no evidence of static spheroidization, but the thickness of alpha lamellas has increased compared to the case when no post-deformation annealing was applied. In areas where there was strain (Figures 8(b) and (d)), the volume fraction of spheroidized grains has increased compared to the as-deformed dynamically spheroidized microstructure and the average diameter of the spheroidized grains has increased, indicating significant static spheroidization has taken place. Comparing the FF (Figure 7(b)) and FR deformation routes (1b and 2b respectively) it can be seen that like in the as-deformed conditions, the fraction of spheroidized grains is higher for FF than for FR. This can be attributed to the greater amount of dynamically spheroidized grains already present, which continue to statically coarsen, and a higher level of stored energy

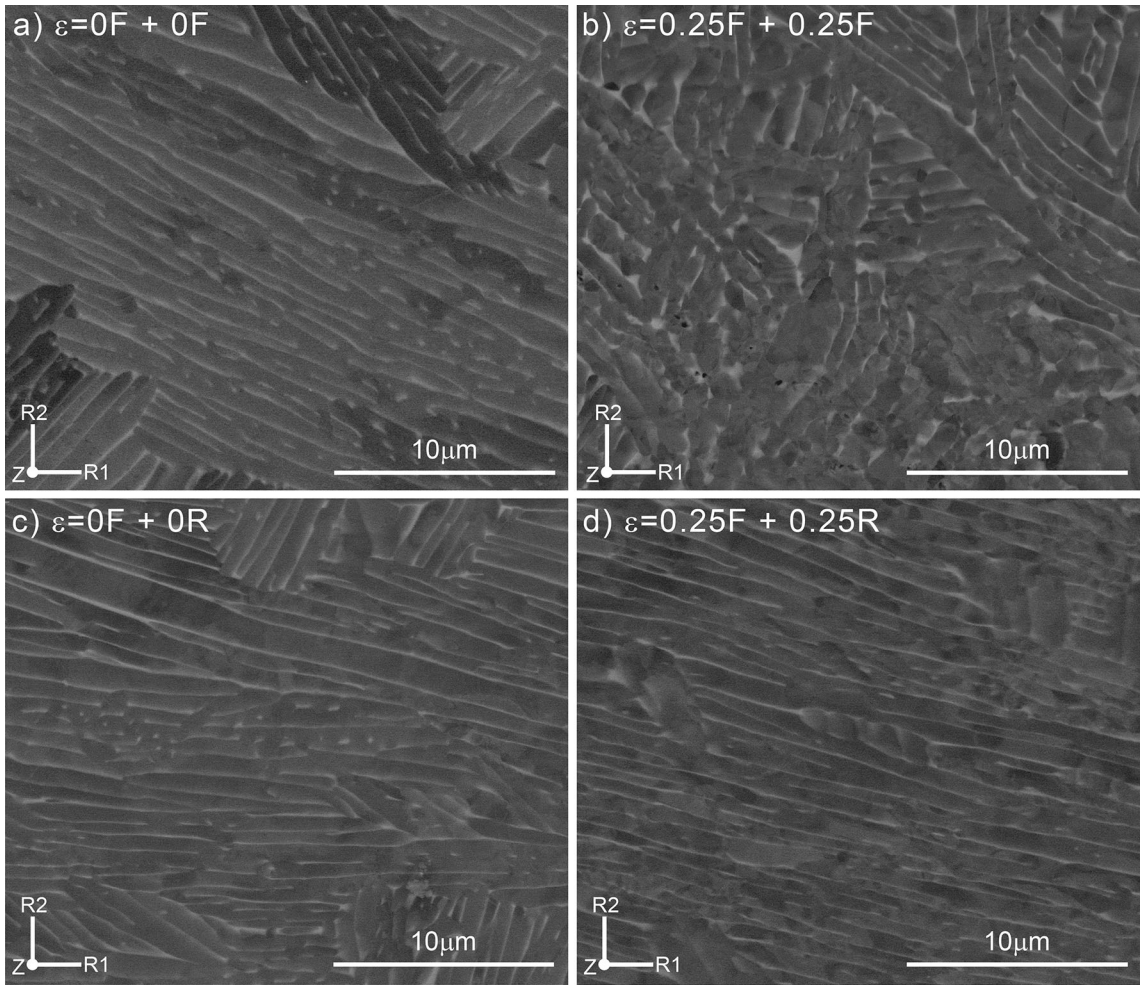

Fig. 5—Micrographs of the deformed specimens obtained using scanning electron microscope with backscatter electron detector: (*a*) sample 1a at total strain of 0, and (*b*) 0.5. (*c*) sample 2a at zero strain, and (*d*) at strain of 0.5.

leading to a greater driving force for static spheroidization of lamella through the above mentioned mechanisms.

A summary of the effect of total strain on the extent of dynamic and static spheroidization from the present study and previous works[4,13] is shown in Figure 9. Dynamically spheroidized fractions of alpha grains are compared for different deformation modes and temperatures (Figure 9(a)). It can be seen that for the tests performed at 1088 K (815 °C) the fraction of alpha spheroidized is much lower when the strain path change is introduced. Furthermore, the results obtained in previous work by other researchers suggested, that there is a monotonic strain that is needed to be exceeded for the rapid completion of the dynamic spheroidization process.[4] It can be seen on Figure 9(a) that after exceeding the monotonic strain of 1, the rate of spheroidization significantly increases and is completed by a strain of 2, however, this behavior is only noticeable for the sample that was monotonically strained. In the case where the strain was reversed, the progress of dynamic spheroidization is lower and the rate of spheroidization is constant and similar to the one during prestraining, leading to incomplete spheroidization. In the current work, the concept of a critical monotonic strain to produce rapid dynamic spheriodization appears to be validated with a montonic strain of about 0.6 required to produce enhanced spheriodization (Figure 7). This lower value critical strain of 0.6 strain compared to a strain of 1 presented by Poths *et al.*[4] is most likely due to the much faster strain rate in this work.

Figure 9 also highlights the difficulty of achieving a spheroidized microstructure for these types of alloys during hot working when only low to medium strains are applied. For example, in the current work for the total strain not exceeding 0.5 even introduction of post-deformation annealing for 4 hours didn't cause full spheroidization (Figure 9(b)). In the case of FF deformation mode only 48 pct of alpha grains were statically spheroidized, whereas in the case of strain reversal less than 10 pct grains were statically spheroidized.

The results presented up to this point confirm that there is a clear effect of strain path on both flow behavior and dynamic and static spheroidization for the applied process conditions. In order to put more insight into understanding these effects, further investigation of the impact of strain reversal on grain shape, orientation,

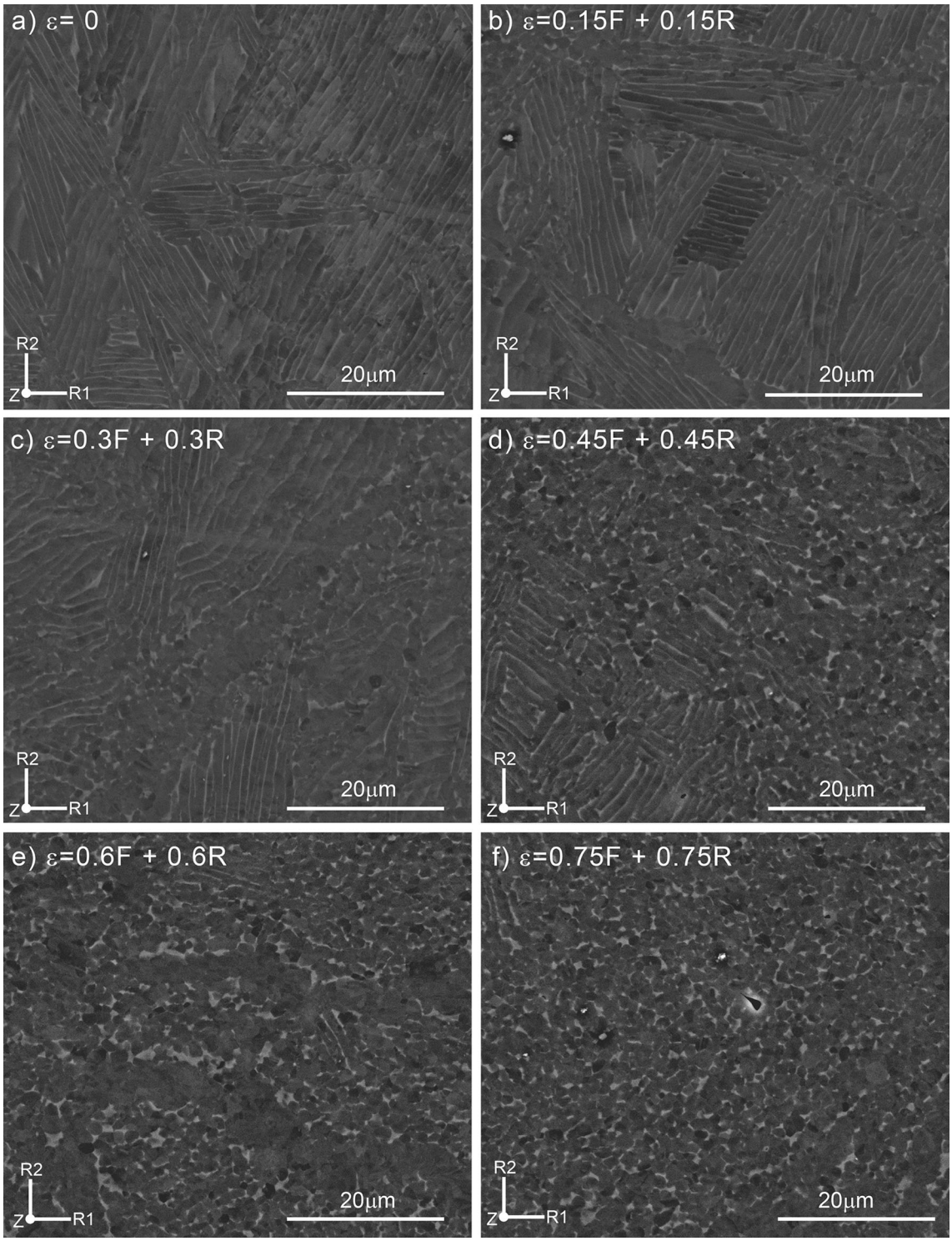

Fig. 6—Illustration of the effect of strain on the progress of dynamic spheroidization in the material deformed according to the deformation route 3.

and misorientation was performed using large area EBSD analysis.

It would be expected that the dynamic spheroidization process leading to complete breakup of the original alpha lamella fully destroys all of the existing Burgers relations between original colony alpha variants within an original beta grain. In order to confirm this thesis, large area inverse pole figure orientation component (IPF) maps were made on the cross sections of the samples from their center to the surface, and are summarized in Figure 10. Due to the deformation gradient within the torsion samples it was thus possible to assess the effect of various strains and strain rates on the microstructure evolution. Figure 10(a) shows the

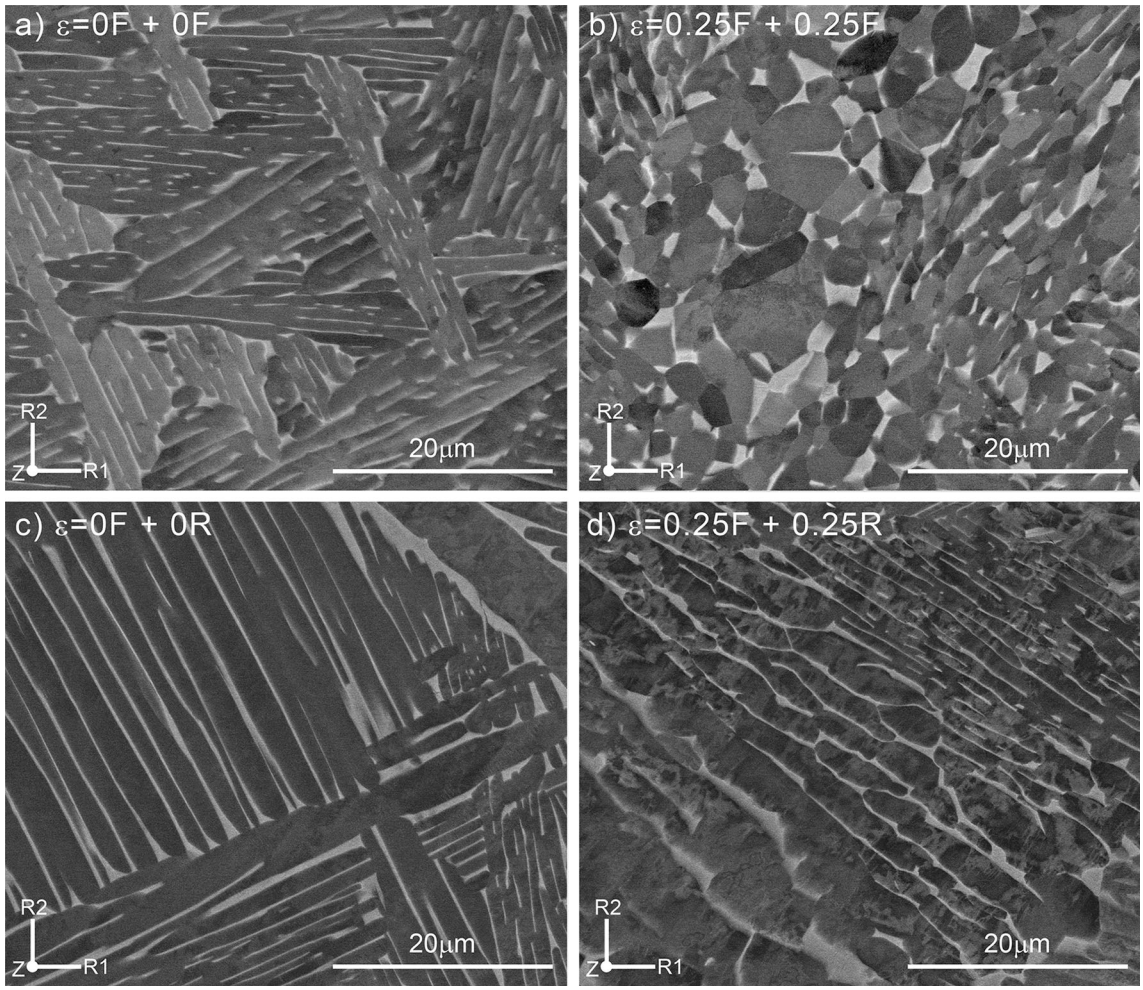

Fig. 7—Micrographs of the deformed and annealed specimens obtained using scanning electron microscope with backscatter electron detector: (*a*) sample 1b at zero strain, and (*b*) strain of 0.5; (*c*) sample 2b at zero strain, and (*d*) at the strain of 0.5.

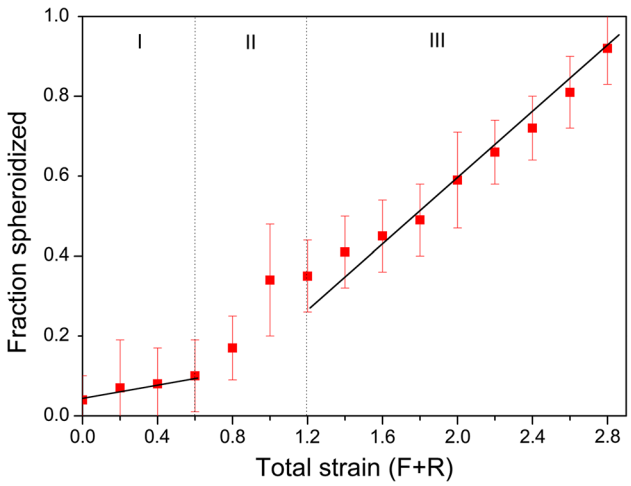

Fig. 8—Fractions spheroidized measured at various positions along radius at the cross section of the torsion sample after deformation route 3. Error bars represent standard deviations.

room temperature microstructure of the as-heat treated sample, whereas Figures 10(c) and (e) show maps measured on specimens deformed according to deformation routes 1a and 2a, respecively. Maps on the Figures 10(b), (d), and (f) show IPF figures of the high temperature beta phase that has been reconstructed using method described in the previous paragraph.

Figure 10(b) shows the reconstructed map of beta phase in the as-heat treated sample. The grain boundaries of the beta phase are indicated by black lines (greater than 15 deg misorientation angle). It can be seen that the reconstruction was possible across the whole area of the sample indicating that the relationship between parent beta phase and inherited alpha phase is valid with respect to the Burgers relationship. Figure 10(d) shows the reconstructed map of the beta grains where the deformation with the FF route was applied (schedule 1a). In this case the prior beta grains were reconstructed only very close to the center of the sample where the strain was close to zero. Beyond this area toward the edge of the specimen's cross section, where both strain and strain rate increase, reconstruction was not possible indicating significant divergence from the Burgers relationship. In the case when the same total strain was applied but the torsion deformation was carried out with a full strain reversal (route 2a), beta grain restoration was successful throughout the sample's

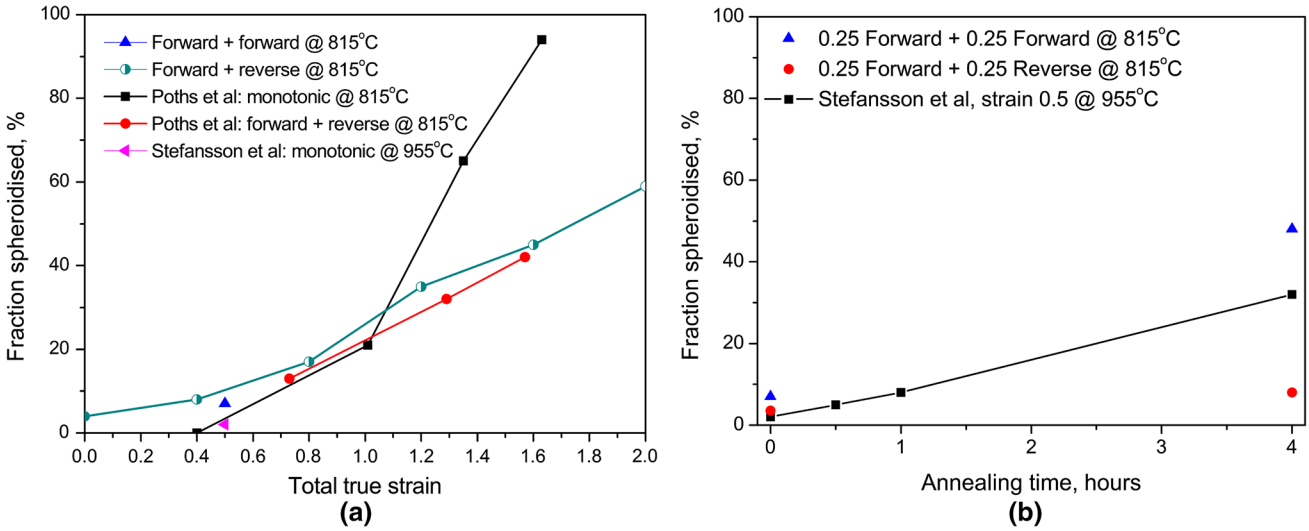

Fig. 9—Effect of strain on the progress of dynamic spheroidization after different strain paths: (*a*) comparison of the current work results with Ref. [4, 13]; (*b*) effect of post-annealing time on the progress of static spheroidization after different strain paths—comparison of the current work with Ref. [13].

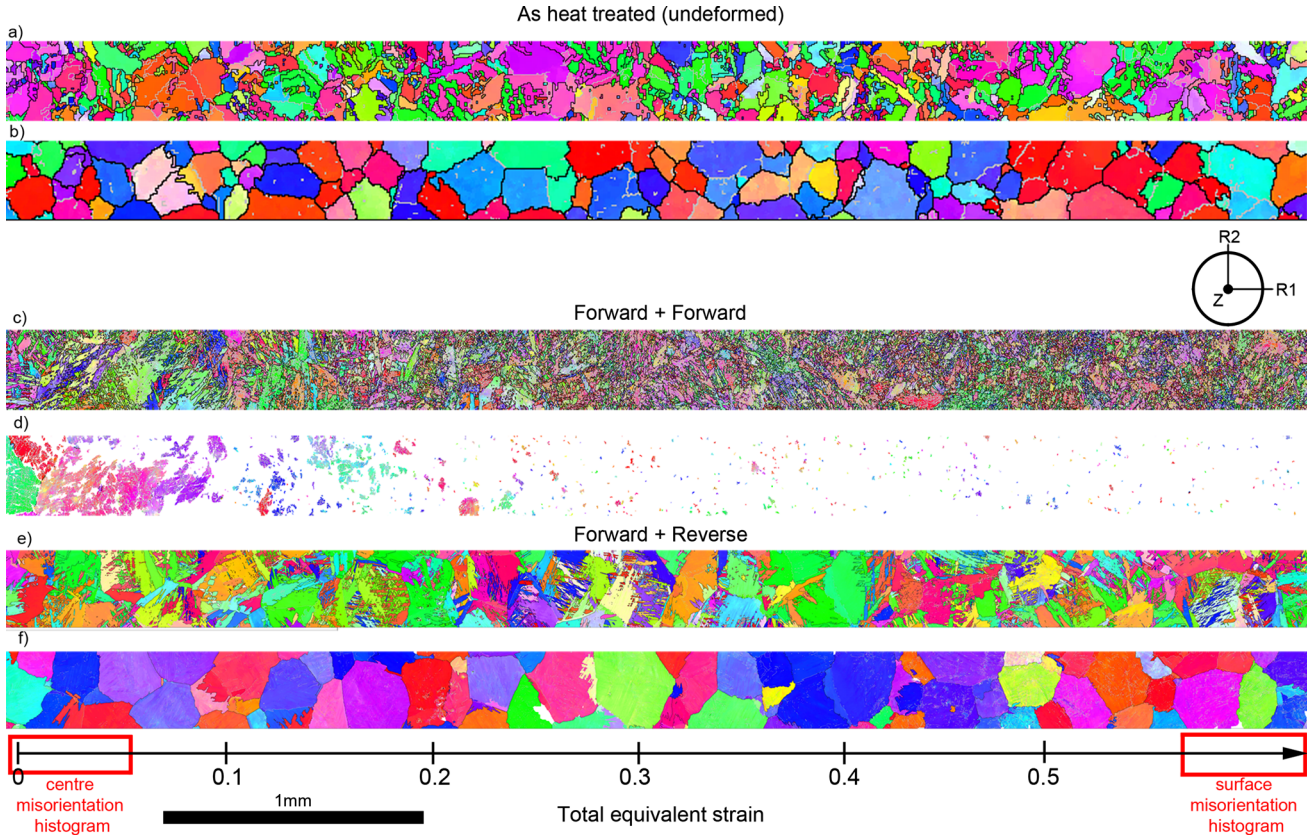

Fig. 10—(*a*), (*c*), (*e*) EBSD maps of alpha grains, and (*b*), (*d*), (*f*) reconstructed beta grains in as- heat treated (undeformed) sample and material deformed according to routes 1a and 2a.

cross section. This indicates that for the applied total strain (0.25 forward 0.25 reverse), the original beta grains have been restored upon the strain reversal. More details about this behavior can be seen in Figure 11. When beta-to-alpha phase transformation occurs, the variants inherited from the same beta grain form different alpha colonies characterized by specific misorientations between them *i.e.*, 10, 60–63, 90 deg.[8] In

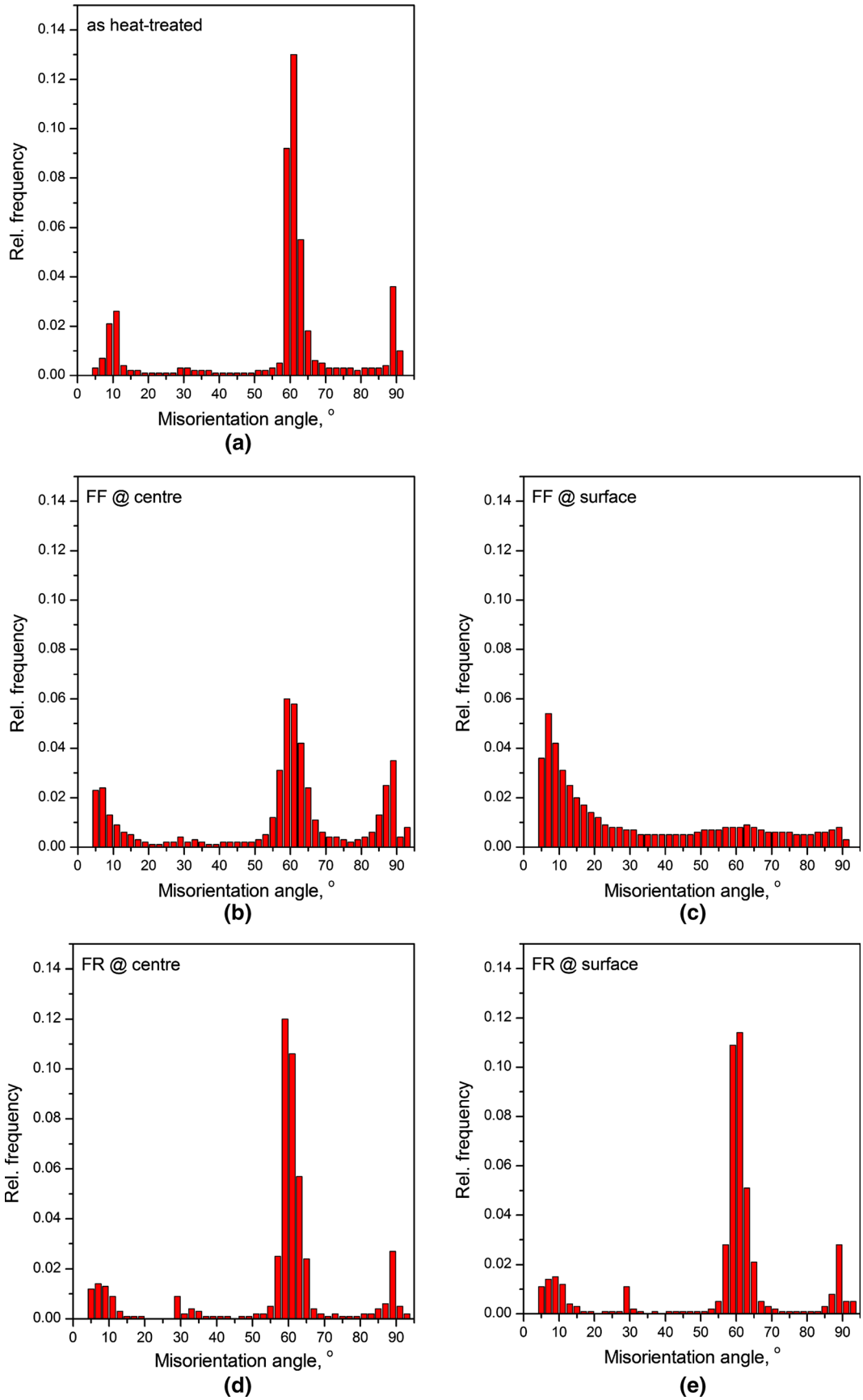

Fig. 11—(*a*), (*b*), (*d*) misorientation angle distribution of alpha grains in the area near the center, and (*c*), (*e*) near the surface of the torsion specimen's cross section after heat treatment only (a) and deformation routes 1a (b, c) and 2a (d, e).

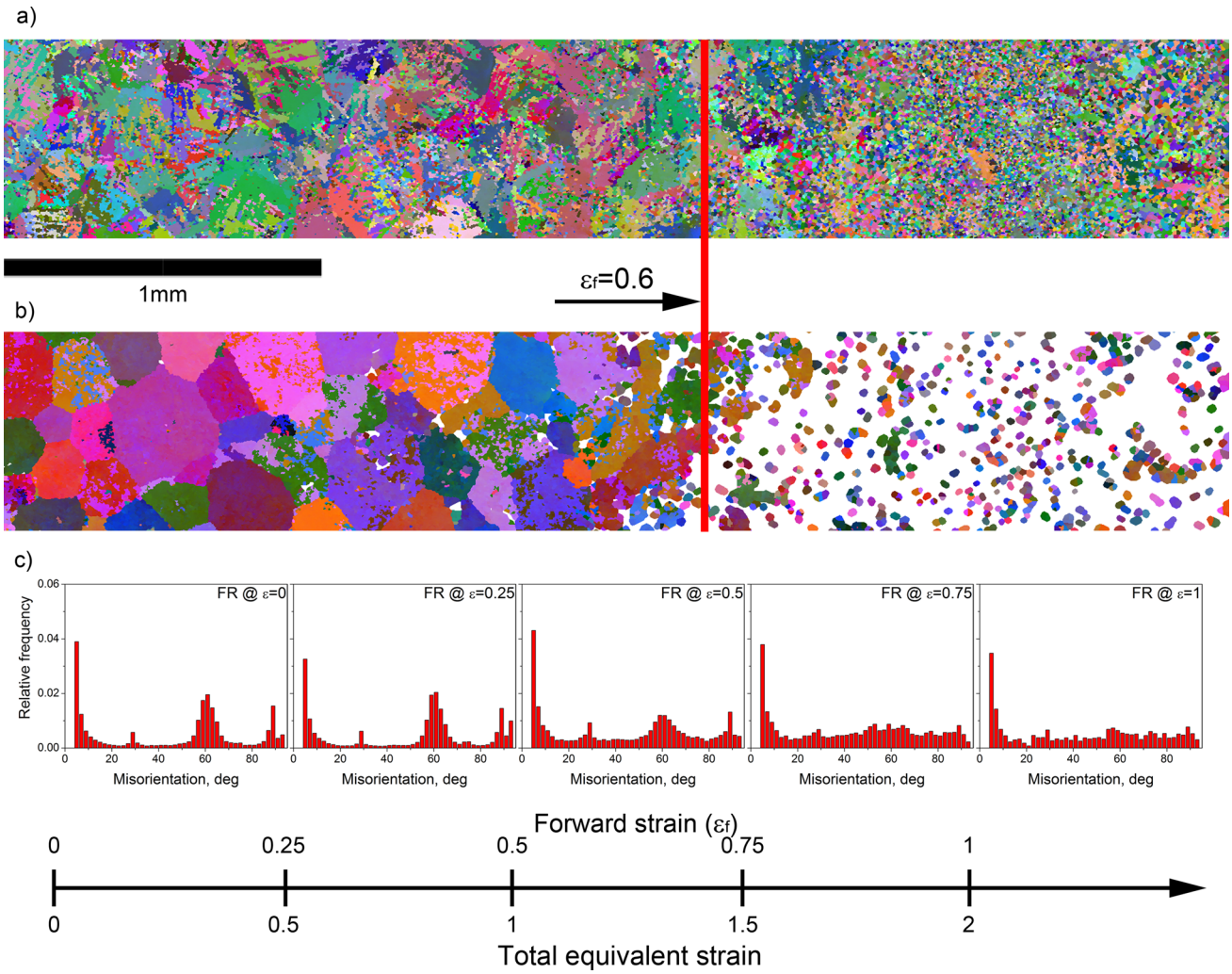

Fig. 12—EBSD maps of (*a*) alpha phase and (*b*) corresponding map of reconstructed beta phase with marked threshold strain for restoration of the original shape of beta grains—specimen deformed with route 3. (*c*) Histograms of grain boundaries misorientation distributions measured locally for corresponding strains.

the as-heat treated sample, the grain boundary distribution, Figure 11(a), shows strong densities around these specific angles corresponding to these strict Burgers misorientation angles between variants.

In the case of as-deformed samples, it can be seen that in the area close to the specimens' centers (Figures 11(b) and (d)), the Burgers relationship is maintained. However, when the misorientation distributions measured at the surface are compared (Figures 11(c) and (e)), it can be noticed that the Burgers relationship is visible only in the case of FR deformation (route 2a). In the case of FF deformation (route 1a) the Burgers relationship has been destroyed. It can be concluded that for the applied total strain of 0.5, full strain reversal led to a fully restored beta structure, whereas in the case of the same total strain applied in monotonic deformation, the restoration of the original beta structure was no longer possible. It should be noted however that at a half radius of the FF sample (which is equivalent to the 0.25 forward strain only) we know that we also have no reconstruction of the beta grains. However, upon strain reversal, the original microstructure at this point was fully reconstructed suggesting that, like in a single phase materials, both grain shapes and their orientations can be fully restored[7] in these multiphase lamella type microstructures. This reversibility would then suggest that morphological changes (spheroidization) have not occurred up to monotonic strain of 0.25.

In order to identify whether there is a threshold monotonic strain, beyond which the reversal of the microstructure is no longer possible, additional experiment was conducted with deformation route 3, where strain of 1 in each pass (total strain of 2, net strain of zero) was applied. In this case, however, the test was carried out at lower strain rate ($0.05\ s^{-1}$) to insure structural integrity of the sample.[14] Results showing EBSD map of alpha phase taken across entire radius on specimen's cross section together with reconstructed beta phase are summarized in Figure 12. It can be seen that in this case beyond the total strain of about 1.2 (0.6F 0.6R) the microstructure appears to be much more

refined suggesting significant morphological change and refinement of the microstructure. Looking at Figure 12(b) it can be noticed that beyond the total strain of 1.2 it was impossible to reconstruct any beta grains. Additionally, it should be noted that even at slightly lower strains, there are areas where reconstruction of beta grains was not complete, suggesting the Burgers relationship in these areas was already destroyed most likely by the onset of dynamic spheroidization. This would suggest that there is a threshold monotonic strain, beyond which the return of the original as-transformed Burgers relationship is no longer possible, similarly to that observed in the microstructure study as discussed above. This is further confirmed by misorientation profiles measured along the radius (Figure 12(c)). Typical Burgers misorientation profiles were obtained only up to this level of strain.

IV. SUMMARY

The effect of strain-path reversal on the dynamic and static spheroidization of the colony-alpha microstructure in alpha/beta titanium alloy was established via torsion testing of Ti-6Al-4V at 1088 K (815 °C) and a strain rate of 0.5 s^{-1}, with two different strain-path histories. The following conclusions may be drawn from this work:

1. Volume fraction of dynamically spheroidized alpha grains is much lower when the strain-path change is introduced. For the first group of tests, where the total applied strain was 0.5, dynamic spheroidization hardly started in both strain path histories. This result highlights the difficulty of achieving a spheroidized microstructure for these type of alloys during hot working.
2. For higher total strains, where there is a strain reversal, three regions where the rate of dynamic spheroidization changes can be identified. A critical monotonic strain in the range of 0.3 to 0.6 was identified that has to be exceeded to initiate rapid spheroidization, which is consistent with the flow data and microstructure observations. The existence of this transitional strain region can be attributed to various alpha colony orientation sensitivity to dynamic spheroidization.
3. Extent of static spheroidization of alpha grains is also significantly affected by the whole thermomechanical history. For the strain applied in the present work, introduction of post-deformation annealing did not cause full spheroidization process. In the case of FF deformation mode, after 4 hours of annealing only 48 pct of alpha grains were spheroidized, whereas in the case of strain reversal less than 10 pct grains were spheroidized. This enhanced level of static spherodization in the case of material after FF deformation can be attributed to the greater amount of dynamically spheroidized grains already present, which continue to statically coarsen, and a higher level of stored energy leading to a greater driving force for static spheroidization of alpha lamella.
4. For the applied total strain of 0.5, full strain reversal led to fully restored prior beta structure, whereas in the case of the same total strain applied in monotonic deformation the original beta structure was destroyed. Also, the crystallographic orientations of the reversed alpha grains were fully restored. For the strain reversal, exceeding monotonic strain of 0.6 no return effect to the original grain shape was observed and Burgers relation was fully destroyed.

REFERENCES

1. S.L. Semiatin, V. Seetharaman, and I. Weiss: *Mater. Sci. Eng.*, 1999, vol. A263, pp. 257–71.
2. S.P. Fox and D.F. Neal: *Proceedings of the 8th World Conference on Titanium, Titanium'95*, P.A. Blenkinsop, W.J. Evans, and H.M. Flower, eds., Institute of Materials, London, 1995, pp. 628–35.
3. A.F. Wilson, V. Venkatesh, R Pather, J.W. Brooks, and S.P. Fox: *The Prediction of Microstructure Development During Timetal 6-4 Billet Manufacture, Titanium*, 2003, pp. 321–28.
4. R.M. Poths, G. Angela, B.P. Wynne, W.M. Rainforth, S.L. Semiatin, and J.H. Beynon: *Metall. Mater. Trans.*, 2004, vol. 35A, pp. 2993–3001.
5. S.L. Semiatin and N. Stefansson: *Metall. Mater. Trans.*, 2003, vol. 34A, pp. 691–98.
6. D.F. Fields and W.A. Backofen: *ASTM Proceedings of the 60th Annual Meeting,* 1957, vol. 57, pp. 1259–72.
7. P.S. Davis: Ph.D. Thesis, The University of Sheffield, Sheffield, UK, 2009.
8. N. Stanford and P. Bate: *Acta Mater.*, 2004, vol. 52, pp. 5215–24.
9. N. Gey and M. Humbert: *Acta Mater.*, 2002, vol. 50, pp. 277–87.
10. D.R. Barraclough, H.J. Whittaker, K.D. Nair, and C.M. Sellars: *J. Test. Eval.*, 1973, vol. 1, pp. 220–26.
11. S.B. Davenport, R.L. Higginson, and C.M. Sellars: *Philos. Trans. R. Soc. Lond.*, 1999, vol. A357, pp. 1645–61.
12. Q. Zhu and C.M. Sellars: in *Proceedings 2nd International Conference on Modelling of Metal Rolling Processes,* London, 9–11 September 1996, J.H. Beynon, P. Ingham, H. Teichert, and K. Waterson, eds., The Institute of Materials, London, 1996, p. 158.
13. N. Stefansson, S.L. Semiatin, and D. Eylon: *Metall. Mater. Trans.*, 2002, vol. 33A, pp. 3527–34.
14. S.L. Semiatin and J.J. Jonas: *Formability and Workability of Metals: Plastic Instability and Flow Locallization*, ASM International, Metals Park, 1984.